Rendezvous design in a cislunar near rectilinear Halo orbit

Emmanuel Blazquez, Laurent Beauregard, Stéphanie Lizy-Destrez, Finn Ankersen, Francesco Capolupo

Rendezvous design in a cislunar near rectilinear Halo orbit

E. Blazquez, L. Beauregard and S. Lizy-Destrez
emmanuel.blazquez@isae-supaero.fr
Institut Supérieur de l'Aéronautique et de l'Espace (ISAE-SUPAERO)
Department of Aerospace Vehicles Design and Control
Toulouse
France

F. Ankersen
European Space Research and Technology Center
Guidance, Navigation and Control Systems
Noordwijk
Netherlands

F. Capolupo
Airbus Defence and Space
Advanced Flight Dynamics, GNC and AOCS Studies
Toulouse
France

ABSTRACT

In the context of future human spaceflight exploration missions, Rendezvous and Docking (RVD) activities are critical for the assembly and maintenance of cislunar structures. The scope of this research is to investigate the specifics of orbits of interest for RVD in the cislunar realm and to propose novel strategies to safely perform these kinds of operations. This paper focuses on far rendezvous approaches and passively safe drift trajectories in the Ephemeris model. The goal is to exhibit phasing orbit requirements to ensure a safe far approach. Ephemeris representations of Near Rectilinear Halo Orbits (NRHOs) were derived using multiple-shooting and adaptive receding-horizon targeting algorithms. Simulations showed significant drift and overlapping properties for phasing and target orbits of interest, motivating the search for safe natural drift trajectories and using impact prediction strategies.

Keywords: Rendezvous; Near rectilinear Halo orbits; CR3BP; Ephemeris; Trajectory design; Safety

NOMENCLATURE

Abbreviation

ATV	Automated Transfer Vehicle
CR3BP	Circular Restricted Three-Body Problem
EML-2	Second Earth-Moon Lagrangian point
GNC	Guidance, Navigation and Control
ISS	International Space Station
NRHO	Near Rectilinear Halo Orbit
RVD	Rendezvous and Docking
TT	Terrestrial Time

Symbols

AR	Aspect ratio
A_d	Amplitude of the drift (for Ephemeris-NRHO orbits)
A_z	Out-of-plane elongation (for CR3BP orbits)
d	Distance between chaser and target
m_i	Mass of the i-th primary
N_{LH}	Receding-horizon parameter
O	Barycenter of the primaries
P_c	Probability of collision
$P_{c,max}$	Maximum probability of collision
r_p	Perilune radius
$r_{p,chaser}$	Perilune radius of the chaser's CR3BP initial reference orbit
$r_{p,target}$	Perilune radius of the target's CR3BP reference orbit
r_i	Distance from the chaser to the i-th primary
R_c	Radius of the chaser
R_t	Radius of the target
T	Period
U	Gravitational potential
U_k	Partial derivative of the gravitational potential with respect to the variable k

Greek Symbols

ΔV	Impulsive velocity increment
ϵ	Numerical tolerance
θ	Mean anomaly
μ	Mass parameter of the CR3BP system
μ_i	Gravitational parameter of the i-th primary
σ	Standard deviation

1.0 INTRODUCTION

A Lunar Orbital Platform Gateway[(1)] concept has been recently proposed by the North American Space Agency (NASA) as a pillar for future missions to the Moon's surface. Such an infrastructure is also expected to take advantage of the complex non-linear dynamics about the Lagrangian points of the Earth-Moon system to facilitate human exploration

beyond the cislunar space. The assembly of this structure is expected to happen on orbit within the next decade, with the launch of the Gateway's first module scheduled for 2022. The platform will need to accomodate modular assembly, cargo delivery and crew exchange operational activities, all of which rely critically on Rendezvous and Docking (RVD) operations with modules such as Orion[2]. There is extensive experience with RVD in the two-body problem in Low Earth and Lunar Orbits to various space stations, based on the Apollo missions or the ATV (Automated Transfer Vehicle) deliveries to the International Space Station (ISS). Despite that, the problem of RVD in non-Keplerian dynamics is quite a recent topic, and no operational rendezvous has yet been performed in the vicinity of the Lagrangian points.

Missions involving the Gateway and the Orion spacecraft have kick-started a new trend of publications and research on proximity operations in the cislunar realm. Near Rectilinear Halo Orbits (NRHOs) have been identified as suitable orbits to host the Gateway and to accommodate multiple mission staging[3]. NRHOs exhibit nearly stable behaviour, offer interesting low-cost accessibility conditions from the Moon and the Earth and present favorable communication opportunities from both the Earth and the Moon. Recently, new low-cost orbit maintenance and navigation strategies have been proposed for such orbits[4]. The exploitation of multi-body dynamics for far and close proximity operations is a very active field of research in the astrodynamics community with recent publications advocating for the use of invariant manifold structures to reduce the costs of RVD operations[5,6].

The scope of this research is to propose novel methodologies and trajectory designs to accommodate the constraints of rendezvous operations between a 'chaser' spacecraft and a 'target' orbiting platform in a non-Keplerian environment. Previous contributions from the authors have investigated traditional multi-body far-approach strategies, as well as close rendezvous dynamics using linear and non-linear targeting algorithms[7]. This paper proposes a new strategy for far rendezvous operations in non-Keplerian environments, focusing on natural far approach, and the investigation of passively safe drift trajectories in the Ephemeris model. The goal is to exhibit phasing orbit requirements, given a prescribed target orbit, which will ensure safe free motion and natural approach of a spacecraft near the target. Such trajectories result in significantly low ΔV budgets to safely reach the vicinity of the target from where to engage in close proximity operations.

2.0 NEAR RECTILINEAR HALO ORBITS IN HIGH-FIDELITY MODELS

2.1 The circular restricted three-body problem (CR3BP)

The CR3BP describes the motion of a massless body P under the gravitational influence of two massive primaries orbiting circularly around their common center of mass, with masses m_1 and m_2, respectively, and $m_1 > m_2$. The mass parameter $\mu = \frac{m_2}{m_1+m_2}$ is introduced. The motion is studied in a barycentric, non-dimensional, rotating reference frame (O, x, y, z) called the synodic frame (depicted in Fig. 1) so that the primaries rotate counterclockwise about their barycentre O and are fixed on the x axis at $(-\mu, 0, 0)$ and $(1-\mu, 0, 0)$, respectively. Libration points, also called Lagrangian points, are the five equilibrium points of the CR3BP depicted in Fig. 2.

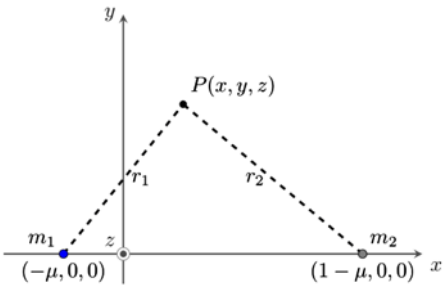

Figure 1. The CR3BP in the synodic frame.

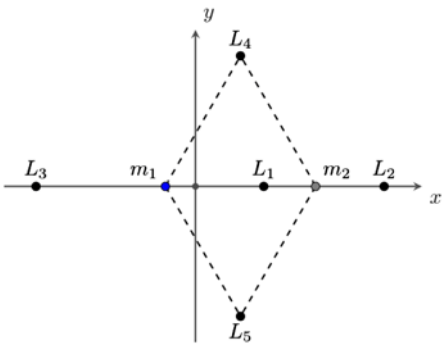

Figure 2. Equilibrium points of the CR3BP.

The differential equations describing the motion of the massless particle P are[8]:

$$\begin{aligned} \ddot{x} - 2\dot{y} &= U_x \\ \ddot{y} + 2\dot{x} &= U_y \\ \ddot{z} &= U_z, \end{aligned} \qquad \ldots (1)$$

where the gravitational potential U can be written as:

$$U(x,y,z) = \frac{x^2+y^2}{2} + \frac{1-\mu}{r_1} + \frac{\mu}{r_2} + \frac{\mu(1-\mu)}{2} \qquad \ldots (2)$$

U_x, U_y and U_z are the partial derivatives of U with respect to x, y and z, respectively, and $r_1 = \sqrt{(x+\mu)^2+y^2+z^2}$, $r_2 = \sqrt{(x-1+\mu)^2+y^2+z^2}$.

2.2 The Ephemeris model

The Ephemeris model describes the motion of a massless body P under the gravitational field generated by $N-1$ massive primaries. The absolute state of the primaries is given by the ephemeris of the precise positions and velocities of the bodies over time in the Earth-centered inertial frame J2000. This frame is defined with respect to the Earth's mean equator and equinox at 12:00 TT on 1 January 2000. Each primary is described by its standard gravita-

Table 1
Gravitational parameters[10]

Primary	μ (km^3/s^2)
Earth	3.9860043623×10^5
Moon	4.902800076×10^3
Sun	$1.32712440040944 \times 10^{11}$

tional parameter μ_i and its absolute position vector $\mathbf{X}_i$ with respect to the Earth. The first primary, described by μ_1, is the Earth. This model is often referred to as the *Restricted Geocentric Solar System N-Body Problem*.

The second-order differential equation describing the evolution of the position vector $\mathbf{X}(t)$ of the massless particle P relative to the position of the first primary, the Earth, in the J2000 frame is[9]:

$$\ddot{\mathbf{X}} = -\mu_1 \frac{\mathbf{X}}{||\mathbf{X}||^3} - \sum_{i=2}^{N-1} \mu_i \left(\frac{\mathbf{X} - \mathbf{X}_i}{||\mathbf{X} - \mathbf{X}_i||^3} + \frac{\mathbf{X}_i}{||\mathbf{X}_i||^3} \right), \quad \ldots (3)$$

where μ_i is the standard gravitational parameter of the i-th primary and $\mathbf{X}_i$ is the position vector of the i-th primary.

The formulation can be modified to take into account additional perturbations, such as the solar radiation pressure or non-uniformities in gravity fields of the primaries. This work will consider a purely Newtonian force model that includes the influence of the Moon, Earth and Sun modelled as point masses using the gravitational parameters shown in Table 1. The states of the primaries are extracted from the DE421[10] Ephemeris of the *Jet Propulsion Laboratory* (JPL), embedded in the SPICE Toolkit.

2.3 NRHOs in the Ephemeris

NRHOs are three-dimensional, periodic orbits of the CR3BP that are a subset of Halo orbits[11,12]. They are characterised by a close perilune passage above one of the Lunar poles and owe their name to their elongated shape (an example is depicted in Fig. 3). They can be identified by their out-of-plane elongation A_z, similarly to other Halo orbits, or more conveniently by their perilune radius r_p with respect to the center of the Moon. It is useful at this stage to define a parametrisation for the location of an object on its reference NRHO orbit. A common choice for a CR3BP NRHO is the θ parameter defined as a fraction of the orbit's period and converted to $[0, 2\pi[$. Such parametrisation can be interpreted as a 'mean anomaly' in the (O, y, z) plane, as shown in Fig. 4. For an Ephemeris NRHO, a similar anomaly can be defined for each revolution of the NRHO as a fraction of the time between the two perilune crossings defining that revolution. Not all locations along the NRHO are suited for close proximity manoeuvers. The perilune region is extremely sensitive to perturbations; impacts of errors and dispersion will therefore be greater[6,7].

This paper will consider exclusively Southern NRHOs about the second Earth-Moon Lagrangian point EML-2 (low-perilune crossing at the North Pole, apolune at the South Pole). Perfectly periodic in the CR3BP, NRHOs loose their periodicity in higher fidelity models. It is possible, however, with regular stationkeeping, to maintain quasi-stable, quasi-periodic motion.

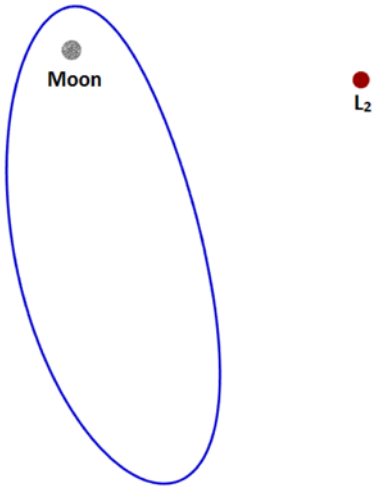

Figure 3. EML2 Southern NRHO with r_p = 5,930km

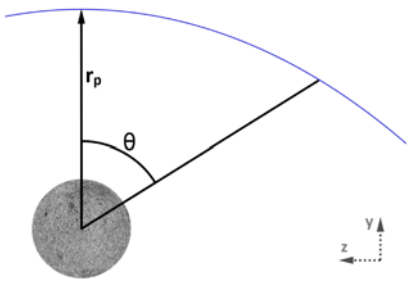

Figure 4. Projection in the (z,y) plane and zoom in the perilune region.

Several steps of corrections are required to efficiently generate long-term NRHO-like orbits in the Ephemeris model:

1. *Generation of the reference NRHO in the CR3BP*
   Usual methods, such as the one chosen in this work, require differentially correcting semi-analytical expansions of solutions obtained via the Lindstedt-Poincaré method[13] to close the orbit by manipulating its perilune state properties. This is further simplified by symmetry properties of Halo orbits that impose perilune and apoapsis states with $\dot{x} = \dot{z} = 0$ at the (O, x, z) plane crossing. The CR3BP reference orbit provides a good initial guess for a correction procedure in the Ephemeris[14,15].
2. *First-level correction of the CR3BP: initial guess in the Ephemeris*
   Firstly, the reference CR3BP NRHO is sampled and directly transitioned to the Ephemeris model. The sampling is performed regularly (at fractions of the orbital period) along the orbit using six patch points. This transition is performed by dimensioning the positions of the state vector by the instantaneous value of the Earth-Moon distance, obtained from the Ephemeris, and dimensioning the velocity components of the state vector by the mean norm of the angular velocity vector over one synodic cycle.

Figure 5. EML2 Southern NRHO with r_p = 5,930km, from multiple-shooting correction, after ∼100 days.

A forward-propagation multiple-shooting correction scheme is then applied to the first guess generated by the sampling and transition of the CR3BP reference. The state components and epochs of the patch points, other than the initial perilune crossing, are control variables of the correction process. In order to ensure time continuity of the converged solution, stringent epoch continuity constraints must be enforced[9]. The correction is performed in the J2000 frame with a threshold of $\epsilon = 10^{-6}$ for non-dimensional state discontinuities at the patch points ($\sim$ 400m in position and 1mm/s in velocity).

Orbits obtained after this first-level correction are stable for $\sim$ 100 days, after which the cumulative patch discontinuities inherent to the multiple-shooting process cause the solution to diverge as showcased in Fig. 5. A second layer of correction is required to improve the stability of the solution and consequently enable long-term propagation.

3. *Second-level correction: adaptive receding-horizon*
   The result from the multiple-shooting correction is used as a first guess for a receding-horizon procedure. The method relies on enforcing the symmetry properties of NRHOs: $\dot{x} = 0$ in the (O, x, y, z) synodic frame at each perilune and apolune crossing. The correction is performed in a pulsating (O, x', y', z') reference frame that can locally be compared to the synodic frame (it is locally defined as the synodic frame at that epoch; the rotation is such that the primaries will always be aligned with the x-axis of such frame). By enforcing $\dot{x}' = 0$ at selected perilune crossings, one ensures that its out-of-plane velocity component remains under control.
   The initial guess is propagated forward in time from its initial $\mathbf{x}'_{\mathbf{p,0}}$ perilune crossing to a further perilune crossing $\mathbf{x}'_{\mathbf{p,k}}$, a number N_{LH} of revolutions downstream. The velocity states $(\dot{x}'_{p,0}, \dot{y}'_{p,0}, \dot{z}'_{p,0})$ are control variables of a single-shooting correction procedure targeting $\dot{x}'_{p,k} = 0$. The orbit obtained is quasi-stable for N_{LH} revolutions. The state is propagated for a single revolution from $\mathbf{x}'_{\mathbf{p,0}}$ to $\mathbf{x}'_{\mathbf{p,1}}$, and the procedure is repeated until stability is guaranteed for the desired amount of revolutions. This process is illustrated in Fig. 6.

This work proposes a novel implementation of an adaptive N_{LH} parameter within the receding-horizon procedure. Empiric data from multiple runs of fixed-parameter receding-horizon procedures applied to Halo orbits showed that values in the $6 < N_{LH} < 10$ range

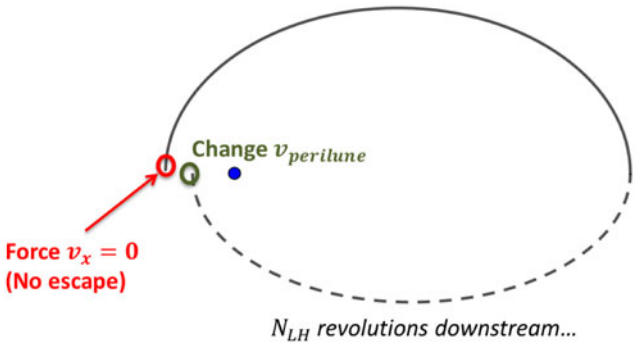

Figure 6. Receding-horizon correction procedure for an NRHO with an N_{LH}-revolutions horizon.

Figure 7. EML2 Southern NRHO with r_p = 5,930km, with receding-horizon correction, 500 revolutions.

offered satisfying results but were highly dependent on the orbit considered and the Sun-Earth-Moon configuration. The N_{LH} parameter can be dynamically selected at each correction iteration by looking at the error projection after the long-horizon propagation and increased or decreased accordingly. One must note, however, that increasing the parameter can lead to higher difficulty to converge because the orbit propagated from the last perilune step is guaranteed quasi-stable only for a number of revolutions inferior to the newly tuned N_{LH}. This phenomena is observed in a specific instance: when N_{LH} approaches the critical value corresponding to $N_{LH} \cdot T \sim 100$ days, usually for 'worst case scenarii' of the Earth-Sun-Moon configuration. In this case, backtracking to previous iteration steps with softening of the increase of the receding-horizon parameters restores proper convergence.

This choice of an adaptive receding horizon-parameter leads to both lower computational strain and station-keeping budgets for orbit maintenance. With this procedure, the maintenance budget for a 500-revolution NRHO orbit with $r_p = 5,930$km (depicted in Fig. 7) is equal to 61.729mm/s with maximum manoeuver amplitude of 0.518mm/s, which represents a slight improvement with respect to previous implementations found in the literature[3].

3.0 NATURAL DRIFT FAR RENDEZVOUS

As an extension of successful rendezvous operations performed in Low Earth Orbit, it is possible to identify three successive phases in rendezvous operations: the transfer phase, the far rendezvous and the close rendezvous. This work focuses on the far rendezvous operations taking place after the spacecraft has been injected into a proper phasing orbit. The term *chaser* refers to the spacecraft performing the manoeuvers to reach the *target* orbiting infrastructure, which was placed on a Southern NRHO about EML2. This section details how to use the natural drift of Ephemeris NRHOs with respect to their reference in the CR3BP to achieve natural far RVD.

3.1 Framework

NRHOs are no longer periodic when translated into the Ephemeris model: both chaser and orbit NRHOs present a significant displacement, or *drift*, with respect to their CR3BP reference in the pulsating frame. The overlapping of chaser and target drifts can be exploited to achieve quasi-free natural far RVD. The scope of this research is to investigate, given a prescribed target NRHO, the perilune radius of nearby chaser NRHOs that allow for natural far RVD. The aim is for the chaser to reach a region of interest in the vicinity of the target from where to initiate relative navigation and close-proximity operations. Such a region will be referred to as the *approach region*, contained within a distance 75km $< d <$ 100km around the target. In the meanwhile, the chaser should avoid entering the *safety region*, defined within a radius of 50km around the target.

In order to classify and select chaser and target orbits according to their natural RVD capabilities, this work defines an *opportunity window* as a portion of the trajectory during which the chaser is within the approach region about the target, outside of the safety region, and satisfies the anomaly constraint $\frac{\pi}{2} < \theta < \frac{3\pi}{2}$ in order to initiate close-approach in near-apolune regions. Within an opportunity window, the chaser is therefore at a distance d with respect to the target satisfying 75km $< d <$ 100km.

The drift of an orbit can be quantified by introducing an amplitude A_d of the drift, in adimensional units:

$$A_d = \max_{\theta \in [0,\ 2\pi[} \| \tilde{\mathbf{X}}(\theta) - \mathbf{x}(\theta) \|, \qquad \ldots (4)$$

where $\mathbf{x}(\theta)$ is the adimensional positional vector of the reference CR3BP NRHO orbit in the synodic frame, at anomaly θ, and $\tilde{\mathbf{X}}(\theta)$ is the adimensional positional vector of the Ephemeris NRHO orbit in the pulsating frame at anomaly θ.

3.2 Candidate search and selection criteria

Different methodologies were used to search for chaser orbit candidates with drifts satisfying the constraints stated in Section 3.1 depending on the precision required and the integration time. As a starting point, an initial set of different candidate orbits are corrected in the Ephemeris model and propagated with $r_{p,chaser}$ within a narrow interval $[r_{p,min},\ r_{p,max}]$ containing $r_{p,target}$. For each propagated chaser orbit, one looks for its number of potential opportunity windows.

From the definition of the amplitude of the drift introduced in Equation 4, a necessary (but not sufficient) condition for a a chaser orbit to offer opportunity windows with respect to the target orbit is:

$$A_{d,chaser} + A_{d,target} \geq \max_{\theta \in [0,\ 2\pi[} \| \mathbf{x}_{chaser}(\theta) - \mathbf{x}_{target}(\theta) \|, \qquad \ldots (5)$$

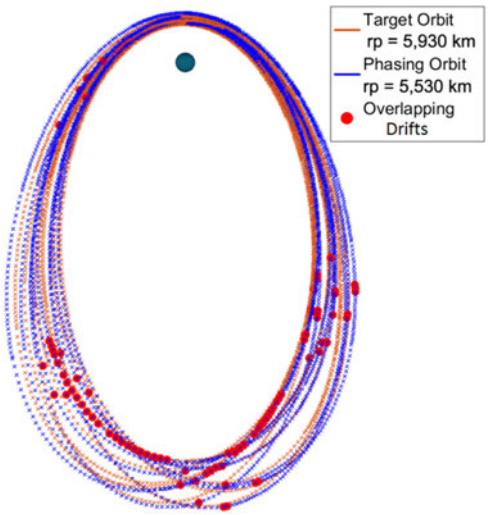

Figure 8. Example of a local plane search procedure for quick feasability assessment.

where $A_{d,chaser}$ and $A_{d,target}$ are the amplitudes of the drifts of chaser and target orbit, respectively; $\mathbf{x}_{chaser}(\theta)$ and $\mathbf{x}_{target}(\theta)$ are the adimensional positional vectors of the reference CR3BP NRHO chaser and target orbits in the synodic frame at anomaly θ. This necessary condition helps when defining a first search interval for $r_{p,chaser}$.

After this initial selection, the first way to find most of the opportunity windows with little computational effort is to apply a local-plane crossing search procedure. For each point of the propagated target orbit, a local plane is defined using its two nearest neighbours. If at some point in the chaser orbit two consecutive states are found on different sides of the nearest local plane of the target orbit, then a single distance check gives information on the dangerosity or interest of the location. Figure 8 showcases such a search performed for a chaser orbit with $r_{p,chaser} = 5,530$km, a target orbit with $r_{p,target} = 5,930$km and neighbours closer than 50km. This method should, however, only serve as a first level feasibility assessment. The search method used to obtain the results presented in this paper uses near-neighbour search implementations coupled with Delauney surface triangulation to refine the search.

In order to further differentiate and select chaser orbit candidates based on their ability to perform natural far RVD with a target orbiting on a prescribed NRHO, a second selection then occurs. Two supplemental criteria are proposed at this stage of the analysis. The first is the duration of the opportunity windows offered by the candidate orbit. Opportunity windows should be long enough to allow for proper assessment of relative dynamics, thruster and sensor orientation and engagement in close proximity operations. The second criterion is the recurrence of the opportunity windows, defined as the time the chaser has to wait in free drift before another opportunity window is reached. Valuable candidates offer opportunity windows with reasonable recurrence times so that in case of a no-go to engage in proximity manoeuvers, the chaser safely drifts away from the target before reaching the next opportunity window within a reasonable time span.

3.3 Safety analysis

The orbits selected for natural far RVD should also be analysed from a safety point of view. Outside of opportunity windows, the presence of the chaser within the safety region defined

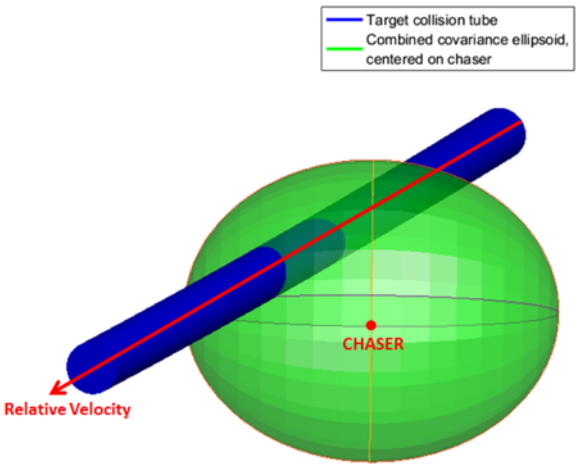

Figure 9. Modelling of an encounter in the approach region.

previously is unavoidable at certain occurrences, notably near the perilune. One must ensure that such events do not present any major risk of collision. The analysis should also be conducted within the approach region to ensure that the trajectory is passively safe. This work uses estimation techniques commonly used for debris-avoidance analyses[16,17].

Chaser and target are both modelled as spherical objects of radii R_c and R_t, respectively. Relative motion is fast enough to be considered linear, and positional noises are zero-mean, Gaussian, uncorrelated. Positional errors of chaser and target are represented by error ellipsoids. Because the uncertainties that define such ellipsoids are assumed to be uncorrelated, co-variances can be summed to build a single combined co-variance ellipsoid centered on the chaser[16]. Collision occurs if the difference in position between chaser and target is less than $R_c + R_t$. The modelling of an encounter within the approach region is shown in Fig. 9.

Instead of using the full integral expression of the probability of collision P_c, this work relies on an expression of a maximum probability of collision $P_{c,max}$[16,17]. For a given aspect ratio $AR \geq 1$ of the projected co-variance ellipsoid in the encounter plane and a given chaser-target distance d, the maximum probability of collision is given by:

$$P_{c,max} = \left(\frac{\alpha}{1+\alpha}\right)\left(\frac{1}{1+\alpha}\right)^{\alpha}, \quad \ldots (6)$$

where

$$\alpha = \frac{(R_c + R_t)^2 AR}{d^2}. \quad \ldots (7)$$

This expression obviously represents an over estimation of the probability of collision (roughly by two orders of magnitudes). It has both the drawback and benefit of being explicitly independent from the co-variance (the dependency is present implicitly in the definition of the projected ellipsoid), and it gives us a useful representation of where the 'wells' for the full probability of collision might be located with damped computational load.

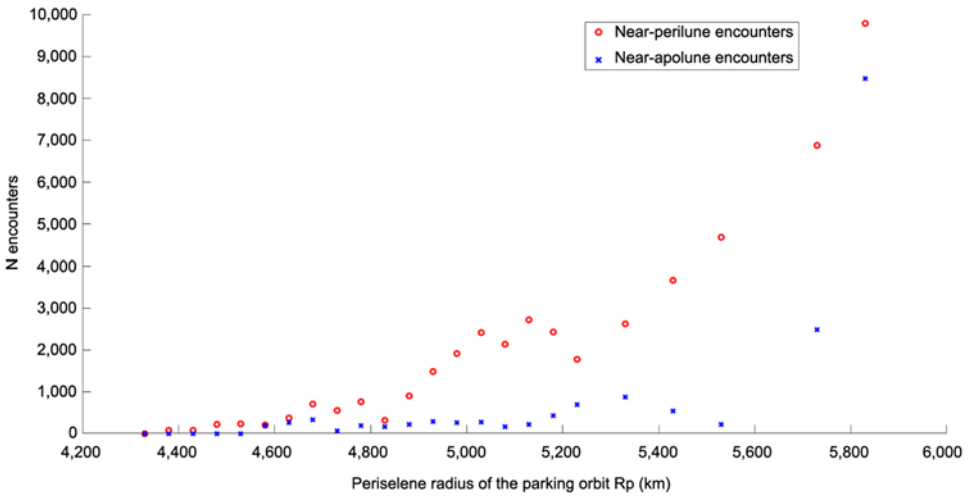

Figure 10. Distribution of encounters in the approach region for different values of perilune radii of the chaser orbit, after ten revolutions of a chaser orbit with $r_{p,target} = 5,300$km.

4.0 SIMULATIONS AND RESULTS

4.1 Study case

A target NRHO with $r_{p,target} = 5,300$km is considered. Such orbit has convenient accessibility constraints[3], low-instability properties and few eclipses due to its 4:1 resonance with the synodic cycle. The chaser is located on an NRHO with varying perilune radius $4,250\text{km} < r_{p,chaser} < 5,900\text{km}$. The reference epoch for orbit generation is set to 8 November 2025 23:22:07. Candidates are analysed for ten target orbit revolutions starting from the reference epoch. For all safety analyses purposes, two different types of error are considered for position dispersion during the encounter: $3\sigma = 1$km (small error) and $3\sigma = 10$km (moderate error). The chaser is modelled as a 10m radius sphere, and the target as a 110m sphere (characteristic dimensions of ATV and ISS, respectively).

4.2 Natural far rendezvous

Figure 10 showcases the distribution of potential near-apolune and near-perilune encounters within the approach region around the target, for varying values of the perilune radius of the chaser reference NRHO, after ten revolutions of the target orbit. Near-apolune encounters will be referred to as *Rendezvous candidates* and are the result of a first selection based on the mean anomaly constraint defined in Section 3.1 and their presence within the approach region.

No encounters happen within the approach region for orbits with $r_{p,chaser} < 4,330$km, and these orbits can therefore be discarded. As $r_{p,chaser}$ tends towards $r_{p,target}$, the number of encounters exponentially grows. This exponential trend is more pronounced for near-perilune encounters. The reasoning at this point is twofold: ensure that the selected chaser orbit reference offers enough encounter opportunities near the apolune and avoid as much as possible perilune encounters that may represent hazardous situations and cannot be selected as RVD locations. For the study case presented in this work, the exponential growth of

perilune encounters skyrockets at $r_{p,chaser} \simeq 5,300$km, and this value should therefore be considered as an upper boundary for the rest of the analysis. No near-apolune encounters occur for phasing orbits with $r_p < 4,550$km: this value represents a lower boundary for chaser orbit perilune radius. The domain under consideration for the chaser orbit is therefore $4,550\text{km} \leq r_{p,chaser} \leq 5,300\text{km}$.

Within this new range, candidate orbits are further analysed and classified according to the properties of their opportunity windows (duration and recurrence), as introduced in Section 3.2. Results for the test case of interest are showcased in Fig. 11, and four different categories are observed based on the value of $r_{p,chaser}$:

1. $r_{p,chaser} \leq 4,750$km: No interesting windows: short durations (maximum of 30 minutes) and a very long wait in between two windows.
2. $4,750\text{km} < r_{p,chaser} < 5,000$km: Within this range, with proper perilune phasing, one can find opportunity windows lasting an average of one hour. However, recurrence is low, and waiting times are long: 100 hours on average. Only one opportunity can be reasonably exploited without considering re-phasing at the next perilune passage.
3. $5,000\text{km} < r_{p,chaser} < 5,100$km: Range best suited for cargo missions: windows last between 1 and 2 hours with typical recurrence times of 23 to 72 hours.
   Example: $r_{p,chaser} = 5,080$km provides 2 opportunity windows lasting 1.08 and 3.45 hours, respectively. The waiting time between both windows is 48 hours.
4. $5,100\text{km} < r_{p,chaser} < 5,300$km: Range best suited for manned missions: windows between 1 and 6 hours, with possibility of recurrence times being less than a day.
   Example: $r_{p,chaser} = 5,230$km provides two opportunity windows lasting 1.03 and 2.13 hours, respectively. The waiting time between both windows is about an hour.

Minimum time between RVD windows within the $5,000\ km < r_{p,chaser} < 5,230\ km$ range is presented in Fig. 11(b). It is important to note, especially for scenarios involving cargo missions, that a re-phasing manoeuver can be performed at the next perilune encounter to accommodate the drift of the orbit and prepare for another window. Because the receding-horizon approach presented in this paper considers perilune maintenance manoeuvers, different passages at the perilune tend to be very close to one another and consequently such phasing manoeuvers have very low orders of magnitude – a few mm/s for the majority of them.

The results presented in this section are sensitive to the choice of initial epoch for the generation of the Ephemeris NRHOs. Variations of the Earth-Moon distance in the Ephemeris model have a predominant impact on the drift observed with respect to the CR3BP reference orbits. By analysing opportunity windows during time spans superior to the Earth-Moon synodic period, one can account for the variation of the Earth-Moon distance and ensure that qualitatively the results will remain similar within one synodic month time frames. However, in order to properly determine the values of $r_{p,chaser}$ corresponding to natural RVD opportunities with a new initial epoch, and in particular to account for the effect of the different Sun phasing, one would need to perform the search again. The general behaviour observed is that durations of opportunity windows tend to shrink when the Earth-Moon system orbits further away from the Sun. This behaviour shall be further investigated and assessed in future research. NRHO injection errors may also result in drift trajectories different from the nominal ones presented in this test case. NRHO injection near the perilune is not recommended in order to avoid large dispersion. If the injection happens in near-apolune regions, in case of dispersion, trajectory correction manoeuvers can be performed at low-cost to re-inject into the nominal trajectory[6,7].

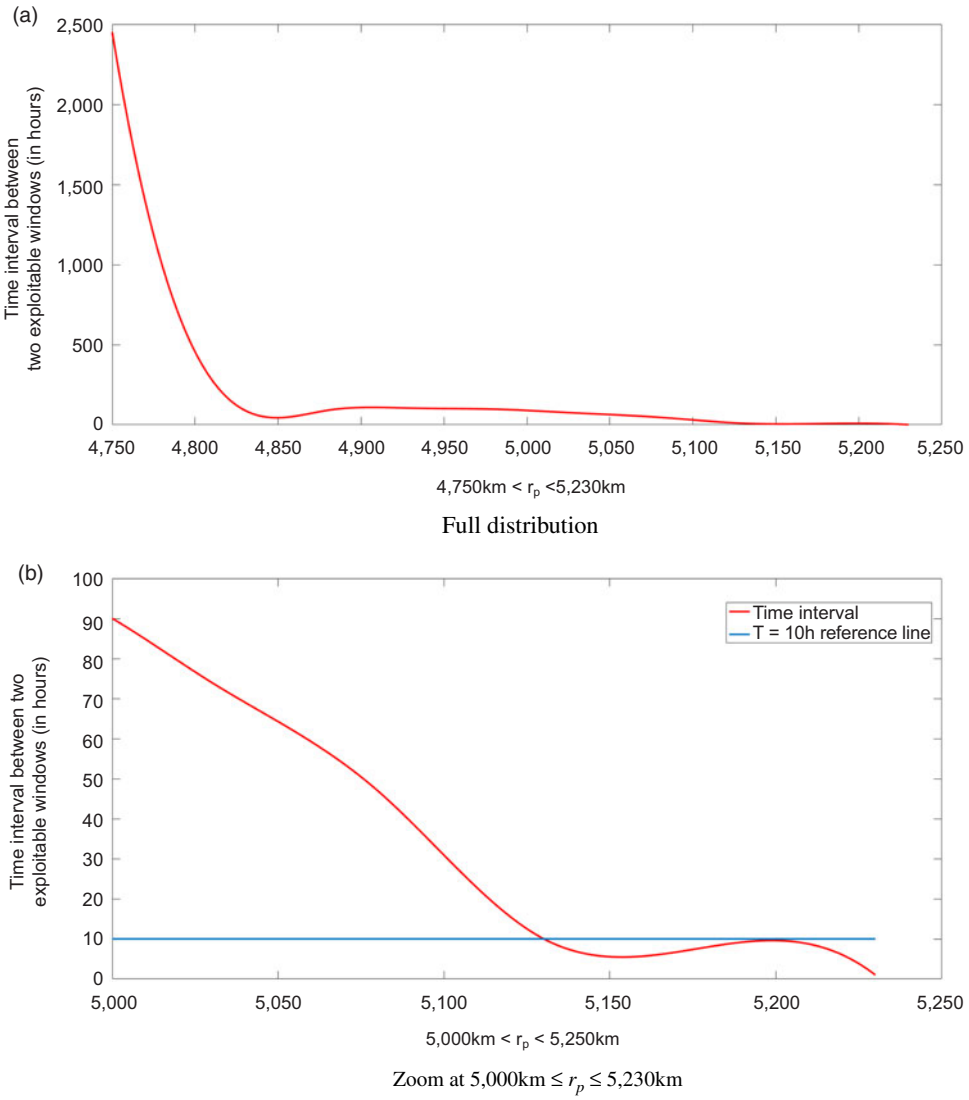

Figure 11. Minimum time between two natural RVD windows.

4.3 Safety analysis

Small state dispersion causes the target to not intersect with the chaser's combined co-variance ellipsoid in the encounter domain, resulting in a quasi-null probability of collision. Moderate dispersion results in the $P_{c,max}$ distribution are presented in Fig. 12. The value $P_{c,max} = 6 \cdot 10^{-4}$ is an absolute threshold that seems reasonable considering the over-estimation of the real probability of collision: it represents a collision event occurring roughly every 450 years. Moreover, some regions of interest to minimise $P_{c,max}$ can be observed around $4,750\text{km} < r_{p,chaser} < 4,950\text{km}$, $r_{p,chaser} \simeq 5,150\text{km}$, and $r_{p,chaser} \simeq 5,250\text{km}$. In such cases, the value of $P_{c,max}$ could therefore be considered as a preliminary safety criteria and contribute to the chaser orbit selection.

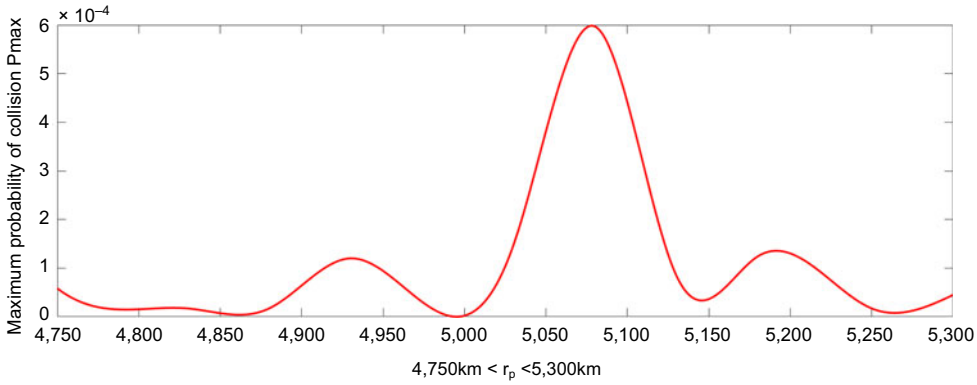

Figure 12. Maximum probability of collision within the safety region for different values of $r_{p,chaser}$.

4.4 Transition to close-proximity operations

After entering the approach sphere, and in case of a 'go' decision, the chaser could engage in relative navigation and start proximity manoeuvers (or 'close rendezvous'[7]). This subject has been the scope of previous work by the authors and is currently investigated. However, one could also complement the natural drift approach with a more traditional trajectory design: a series of impulsive manoeuvers within the approach region to further approach the target and make the transition to close-rendezvous at a closer relative distance. Two scenarios were considered for this transition:

- *Direct transfer:* Lambert's arc in the CR3BP[18], at the end of the drift, targeting the target in its reference NRHO. The CR3BP trajectory is then transitioned to the Ephemeris model using a multiple-shooting procedure similar to the one described in Section 2.3.
- *3-burn low-energy trajectory:* Exploiting the invariant manifolds of chaser and target orbits with a Lambert's arc to connect the manifold branches. The chaser travels along the unstable manifold of its reference NRHO until it reaches the vicinity of a stable manifold branch of the target orbit. The branches are patched using a Lambert's arc in the CR3BP. The trajectory is computed using a Genetic Algorithm for global optimum search, later refined by a gradient-based search. The trajectory in the CR3BP is then transitioned to the Ephemeris model and corrected using a multiple-shooting procedure similar to the one described in Section 2.3.

The Lambert's arc strategy requires a velocity budget between 1 and 20m/s for transfer durations between two and four hours, depending on the location of the natural drift approach zone (regions near the apolune require more ΔV, an order of magnitude more roughly). The manifold-to-manifold methodology has more stringent constraints because the approach region is quite close to the target. The optimal solution of such transfer tends towards the pure Lambert's arc solution with very marginal savings in terms of ΔV and slightly higher time of flights (one to two hours, increases for near-apolune locations). One possible solution to reduce the ΔV budget, at the expense of higher time of flight, is to change the definition of the approach region for the drift and engage the manifold-to-manifold transfer earlier.

It is worth noting that most of the ΔV budget appears when transitioning the trajectories from the CR3BP to the Ephemeris. The optimisation method combining evolutionary global search and gradient-based local search provides very energy-efficient results, which

are severely downgraded by the multiple-shooting procedure. This phenomenon is interpreted to be a consequence of the drift of the trajectory with respect to its CR3BP counterpart that is used for the trajectory computations. The choice of a new reference CR3BP NRHO at the end of the drift could improve the first guess necessary for the transition procedure and therefore reduce the ΔV budget. How to select the new reference NRHO is an open question and should be explored in future research.

5.0 CONCLUSION

This work has presented a novel strategy to design natural drift trajectories in service of far rendezvous operations. The successive steps presented in this paper form a robust methodology to construct quasi-free transfers between NRHO-like orbits in the Ephemeris model with different possibilities to engage the transition to close-proximity operations. Frequent encounter opportunities are feasible, provided careful selection of the chaser orbit's properties with waiting times that can be suitable for both manned and cargo flights. A preliminary safety analysis demonstrated that the risk of collision for such operations is very low and can be further damped. Future research will be oriented towards direct transition to relative navigation within the approach region, at the end of the drift, and the design of a Guidance, Navigation and Control (GNC) system suited to these kinds of operations. The evolution of natural drift trajectories in more perturbed models (Moon's spherical harmonics, solar radiation pressure, etc.) shall also be investigated.

ACKNOWLEDGEMENTS

The authors wish to thank Olivier Mongrard from the European Space Agency (ESA) as well as Joël Bordeneuve-Guibé and Nathanaël Tepakbong-Tematio from Institut Supérieur de l'Aéronautique et de l'Espace (ISAE-SUPAERO) for supporting this work, which was funded under ESA's Network Partnering Initiative in collaboration with Airbus Defence and Space.

REFERENCES

1. Gates, M., Barrett, M., Caram, J., Crable, V., Irimies, D., Ludban, D., Manzell, D. and Ticker, R. Gateway power and propulsion element development status, *69th International Astronautical Congress*, October 2018.
2. Lizy-Destrez, S. Rendezvous optimization with an inhabited space station at EML2, *25th International Symposium on Space Flight Dynamics, ISSFD*, October 2015.
3. Williams, J., Lee, D.E., Whitley, R.J., Bokelmann, K.A., Davis, D.C. and Berry, C.F. Targeting cislunar Near Rectilinear Halo Orbits for human space exploration, *27th AAS/AIAA Space Flight Mechanics Meeting,* February 2017.
4. Davis, D., Sagar, B., Howell, K., Jiang, J.W., Whitley, R., Clark, F., Guzetti, D., Zimovan, E. and Barton, G. Orbit maintenance and navigation of human spacecraft at cislunar Near Rectilinear Halo Orbits, *27th AAS/AIAA Space Flight Mechanics Meeting,* February 2017.
5. Ueda, S., Murakami, N. and Ikenaga, T. A study on rendezvous trajectory design utilizing invariant manifolds of cislunar periodic orbits, *AIAA Guidance, Navigation, and Control Conference,* January 2017.
6. Bucci, L., Colagrossi, A. and Lavagna, M. Rendezvous in lunar near rectilinear Halo orbits, *Advances in Astronautics Science and Technology,* September 2018, **1,** (1), pp 39–43.
7. Lizy-Destrez, S., Beauregard, L., Blazquez, E., Campolo, A., Manglaviti, S. and Quet, V. Rendezvous strategies in the vicinity of the Earth-Moon Lagrangian points, *Frontiers in Astronomy and Space Science,* January 2019, **5,** (45), pp 1–19.

8. Koon, W.S., Lo. M.W., Marsden, J.E. and Ross, S.D. *Dynamical systems, the three-body problem and space mission design,* 2017, Springer-Verlag, New York, pp 26–34.
9. Pavlak, T.A. Trajectory design and orbit maintenance strategies in multi-body dynamical regimes, PhD Thesis, *Purdue University,* May 2013.
10. Folkner, W.M., Williams, J.G. and Boggs, D.H. The planetary and lunar Ephemeris DE421, *Interplanetary Network Progress Report,* August 2009, Tech. Report. Vol. **178**.
11. Howell, K.C. and Breakwell, J.V. Almost rectilinear Halo orbits, *Celestial Mechanics and Dynamical Astronomy,* January 1984, **32,** (1), pp 29–52.
12. Howell, K.C. and Breakwell, J.V. Three-dimensional, periodic, 'Halo' orbits, *Celestial Mechanics and Dynamical Astronomy,* January 1984, **32,** (1), pp 53–71.
13. Richardson, D.L. Analytic construction of periodic orbits about the collinear points, *Celestial Mechanics and Dynamical Astronomy,* October 1980, **22,** (3), pp 241–253.
14. Parker, J.S. and Anderson, R.L. Low-energy lunar trajectory design, 2011, John Wiley & Sons, Hoboken (New Jersey), pp 67–74.
15. Alessi, E.M., Gomez, G. and Masdemont, J.J. A methodology for the computation of constrained orbits and its application to the design of Solar System trajectories, *Journal of the Astronautical Sciences,* 2012, **59,** pp 477–501.
16. Chan, F.K. Spacecraft collision probability, 2008, The Aerospace Press, El Segundo (California).
17. Alfano, S. and Oltrogge, D. Probability of collision: valuation, variability, visualization and validity, *Acta Astronautica,* 2018, **148,** pp 301–316.
18. Topputo, F., Vasile, M. and Bernelli-Zazzera, F. Earth-to-Moon low energy transfers targeting L_1 hyperbolic transit orbits, *Annals of the New York Academy of Sciences,* 2005, **1065,** (1), pp 55–76.